R. & M. No. 3357

R. & M. No. 3357

MINISTRY OF AVIATION

AERONAUTICAL RESEARCH COUNCIL
REPORTS AND MEMORANDA

Measurements of Aerodynamic Heating on a 15° Cone of Graded Wall Thickness at a Mach Number of 6·8

By J. G. Woodley

LONDON: HER MAJESTY'S STATIONERY OFFICE
1964
PRICE 11*s.* 6*d.* NET

Measurements of Aerodynamic Heating on a 15° Cone of Graded Wall Thickness at a Mach Number of 6·8

By J. G. WOODLEY

COMMUNICATED BY THE DEPUTY CONTROLLER AIRCRAFT (RESEARCH AND DEVELOPMENT), MINISTRY OF AVIATION

*Reports and Memoranda No. 3357**
October, 1962

Summary.

This report describes transient wall temperature measurements made on a 15° total-angle cone at zero incidence in an airstream of Mach number 6·8.

The skin of the model was sufficiently thin to allow it to reach zero-heat-transfer conditions within a running time of one minute.

In order to reduce effects of longitudinal heat conduction during a run the electro-formed nickel skin of the model was made with graded thickness, and as a result fairly uniform temperature distributions along the surface were obtained at all times in both the laminar and turbulent regions.

Values of heat transfer, calculated from the wall temperature-time histories using the thin-wall 'heat pulse' assumption, together with recovery temperature are compared to theoretical estimates using the intermediate enthalpy method[10, 11].

LIST OF CONTENTS

* Replaces R.A.E. Tech. Note No. Aero. 2847—A.R.C. 24 447.

LIST OF CONTENTS—*continued*

LIST OF APPENDICES

LIST OF ILLUSTRATIONS

1. *Introduction.*

A very successful method of measuring aerodynamic heat transfer to bodies under transient heating conditions is by the 'heat pulse' technique. For this system the wall of the body must be 'thermally-thin' to the heat pulse applied. This requires that it must be thin enough for a fast temperature response, with the temperature gradients produced through it relatively small, and hence the temperature on the inside surface of the skin close to that on the outside surface. In such cases it is permissible to monitor the wall temperature on the inside surface of the skin and to calculate the aerodynamic heating from its rate of change with time.

For accuracy in the above method the location at which measurements are made must also be 'thermally-isolated', in the sense of being sufficiently remote from odd thermal sources or sinks. However, the fact that a thin wall is used ensures minimum cross-section areas to limit heat conduction to regions in the neighbourhood, and goes some way to reduce such errors.

Even with the above precautions, since in general the aerodynamic heating to a body varies significantly along its length, errors due to heat conduction may still prove to be significant. For this reason heat-transfer measurements to complex model shapes in an intermittent wind tunnel are usually made during the first few seconds of a run, before conduction has had time to distort appreciably the wall temperature distribution. The heat transfer can thus be calculated for an almost isothermal wall by the device of taking the 'initial slopes' of the wall temperature variation with time. The desired levels of wall temperature can then be predetermined by suitable preheating or cooling of the model.

For shapes where the variation of aerodynamic heating along the surface can be predicted reasonably well *a priori*, it is possible to go one step further and actually grade the wall thickness appropriately at each point to ensure approximately uniform warm up of the surface. Thus conduction effects can be minimised and larger running times tolerated.

In order to check this latter technique and at the same time provide basic values of aerodynamic heat transfer for a large range of isothermal wall conditions (a state which is ideally assumed in almost all boundary-layer solutions), a sharp 15° total-angle cone of graded thickness was made from nickel by electro-forming. This was then tested at zero incidence in the $M = 6{\cdot}8$ airstream of the 7 in. × 7 in. Hypersonic Wind Tunnel at the Royal Aircraft Establishment, Farnborough. The assumption of a laminar boundary layer and the requirement that the model should operate from room temperature to an appropriate recovery temperature with a time constant of about 10 seconds fixed the dimensions of the graded wall in this case.

2. *Tunnel and Models.*

2.1. *Tunnel.*

The tests were made at a Mach number of 6·8 in the 7 in. × 7 in. Hypersonic Wind Tunnel at R.A.E., Farnborough. Details of the tunnel design and its performance at this Mach number are given in Refs. 1, 2 and 3.

2.2. *Pressure Model.*

This model was a sharp stainless-steel cone of 15° total angle, which had a length of 15 inches and a uniform skin thickness of 0·1 inches. Pressure holes 1 mm in diameter were placed at approximately 1·5 inch intervals along the top and bottom generators.

2.3. *Heat-Transfer Model.*

Details of this model are illustrated in Fig. 1. In order to obtain a fast response and uniform warm up of the model to avoid longitudinal heat-conduction effects, the cone was made with a thin nickel skin of graded thickness. The model was designed for testing at zero incidence with a laminar boundary layer over the whole of its length. As is shown in Appendix I, this required that the skin thickness of the cone should vary inversely as the square root of the distance from the tip.

2.3.1. *Manufacture of the cone.*—The thin shell of this model was made by electro-depositing nickel in excess onto a former of stainless steel. Final shaping of the nickel model was then made by grinding it to the required sharp conical form whilst still attached to the mandrel. The conical shell was then released from the former by applying pressure circumferentially at its base.

2.3.2. *Accuracy of the model.*—The mean skin thickness variation actually obtained by this method of manufacture for the particular cone used in the present tests is shown in Fig. 2a, and is compared to the design thickness in Fig. 2b. In the latter diagram it should be noted, however, that an error of 10% from design thickness for positions on the surface beyond about 4 inches from the tip results from a discrepancy of only half a thousandth of an inch, which is of the same order as the tolerance to which the diameter of the stainless-steel former itself was manufactured.

3. *Test Conditions and Measuring Techniques.*

3.1. *Test Conditions in 7 in. × 7 in. Hypersonic Tunnel.*

During the tests the stagnation pressure was constant at about 51 atmospheres. The stagnation temperature on the other hand varied with running time, due to heat losses from the airstream in the pipework system before reaching the tunnel settling chamber[3]. A plot of this variation is given in Fig. 3a, and from this it can be seen that stagnation temperature does not begin to steady-out until after 5 seconds or so.

Fig. 3b shows the change in Reynolds number per foot on the cone and in the free stream due to this lag in total temperature. Here once again, as would be expected, comparatively settled values of Reynolds number do not occur until after 5 seconds of the run have elapsed.

3.2. *Measuring Techniques.*

3.2.1. *Stagnation temperature and pressure.*—The methods used for measuring stagnation temperature and pressure are given in detail in Ref. 1.

For the present tests the stagnation pressure was held to within $\pm 0{\cdot}5$ p.s.i. at a level around 765 p.s.i. (abs.) and was measured to an accuracy of $0{\cdot}01\%$ with respect to fluctuations in pressure control to the heater. However, overall accuracy was limited to that of the dead-weight tester (pressure standard) in the measuring system, and was therefore only of the order of $0{\cdot}1\%$.

3.2.2. *Static pressure.*—Static pressures were measured by the electromanometer system described in Appendix II and illustrated in Fig. 4. Accuracy of measuring pressures on the cone by this method is of the order of 1%.

3.2.3. *Wall temperature and heat transfer.*—Wall temperatures were measured at the inside surface of the skin of the model by means of nickel/constantan thermocouples, which were formed by spot-welding constantan wires to the nickel wall. In order to reduce heat conduction from the wall through the thermocouple wires, since the skin thickness itself was only of the order of a

few thousandths of an inch, constantan wires of only one thousandth of an inch in diameter were attached to the skin, being then joined a short distance from the surface to wires of the same material five thousandths of an inch in diameter.

The system used for monitoring the outputs from the thermocouples is illustrated in Fig. 5. Apart from measuring e.m.f. outputs directly on Speedomax (potentiometer) chart recorders[7] to obtain absolute-temperature reference levels, Galvanometer recorders[8] were also used together with 'twin' thermocouples at some stations to monitor the differences in temperature from these reference values at nearby points on the model. This method of iteratively obtaining skin temperatures along the model by use of galvanometer circuits allowed a fair degree of accuracy in the system, since each circuit was individually required to measure only a small temperature difference and could therefore be accurately calibrated. In fact the temperature difference in these circuits could be read to an accuracy of 1°C, which is of the same order as the accuracy to which the reference temperatures monitored on the Speedomax recorders were known.

As is indicated in Appendix II the skin thickness of the model could be correctly described as thermally thin, in as much as the inner and outer wall temperatures would not differ more than $\frac{1}{5}$°C throughout a run. Heat transfer was therefore calculated by equating the convective heat transfer to the rate of increase of thermal energy in the skin. {Equation (3) Appendix I.} For this, longitudinal heat conduction, thermal-radiation effects, and heat losses to the model interior were neglected. The effects that these neglected terms could have had on the results are discussed in Appendix III.

The percentage inaccuracy of the heat-transfer results, obtained in this way from the temporal rate of change of wall temperature, necessarily increases as the run proceeds and the heat transfer to the surface approaches zero. For this reason in the present tests heat-transfer results on the cone are of little interest in the laminar region beyond 30 seconds, and in the turbulent region beyond 20 seconds or so from the start of the run, since in both cases the inaccuracy of the results becomes greater than 10% at further times.

4. *Results and Discussion of Tests.*

All tests were made with the cone models at zero incidence to the airstream at a Mach number of 6·8. The heat-transfer results in fact derive from a single run of 60 seconds duration, since most of the very fine thermocouple wires (Section 3.2.3 and Fig. 5) broke off from the model as it cooled back to room temperature.

4.1. *Pressure Distributions along the Top and Bottom Generators of the Cone.*

Although the pressure model was a few inches longer than the corresponding heat-transfer model, it was in fact mounted in the tunnel with its tip in the same position as the heat-transfer model. Pressure distributions obtained on the top and bottom generators of the cone are shown in Fig. 6. As can be seen the pressure distributions (ratioed to tunnel stagnation pressure p_0) agree reasonably well and the pressures are fairly uniform over the first twelve inches from the tip, which is the region of the working section occupied by the heat-transfer model during testing.

Since at the conical shock wave the flow undergoes an appreciable loss of total pressure, the pressure ratios shown cannot be directly related to a Mach number distribution by the standard isentropic compressible-flow expressions. All that can be done is to use the inviscid solutions from the M.I.T. Cone Tables[9], and compare the experimental pressure ratios obtained with the corresponding Mach numbers on the cone and in the free stream which would in theory give these

ratios. However, as can be seen from Fig. 6, the results are sufficiently close to the free-stream Mach number of 6·8, which was the value found when the tunnel was calibrated, for this and the corresponding Mach number 5·88 on the cone to be representative in order to perform calculations to predict heat transfer to the model.

4.2. *Wall Temperature Distributions—Effect of Transition.*

The wall temperature-time histories obtained at the various stations along the top generator of the cone are shown in Fig. 7. Although no absolute measurement of temperature was made along the bottom generator, comparisons were obtained between various stations on this generator using the Galvanometer circuits (described in Section 3.2.3) alone, without the reference temperature level from Speedomax recorders. The results for the differences in temperature obtained in this way showed approximately the same trends as occurred at comparable stations on the top generator.

Plots, from the curves of Fig. 7, are given in Fig. 8 of wall temperature *versus* distance from the cone tip at various times. As is clearly seen from these and the curves of Fig. 7, at a particular instant during the run the wall temperature is reasonably uniform for the first 4 inches and then increases steadily over the next 2 inches or so to a new fairly uniform level. This strongly indicates that transition of the boundary layer from a laminar to a turbulent state did in fact occur in a region 4 inches or so from the cone tip. Results occurring in the region 4 inches to 6 inches might therefore appropriately be described as transitional.

That this was the state of the boundary layer for the last part of the run (i.e. beyond 40 sec from start of run when conditions are close to zero heat transfer) is clearly indicated in Fig. 7 by comparison with the 'enthalpy' recovery factors, which were obtained at the various stations assuming that the Mach number, M_e, along the cone was 5·88 (the validity of this assumption was considered in the previous section). Here stations downstream of the 6 inch position exhibit turbulent recovery factors of the order of 0·88 whereas upstream of the 4 inch station a recovery factor close to 0·827 is obtained. The latter factor is in fact identical to that which is found by taking Prandtl number to the half power at intermediate enthalpy conditions for the recovery factor as recommended in Refs. 10 and 11 for a laminar boundary layer. In view of the effect on the results due to thermal radiation discussed in Appendix III, this close agreement between theory and experiment is probably somewhat fortuitous.

Since it was not possible to make simultaneous observation of transition on the model during the heat-transfer test, the longitudinal distributions of wall temperature provide the only guide to its position. Several factors which should have had marked influence on its location at each instant are:

(i) The sharp fall in Reynolds number per foot near the start of a run (Fig. 3b), which would be expected to induce a rearward movement of transition as time increased.

(ii) The rise of wall temperature with time would have an increasingly adverse effect on the stability of the boundary layer, with the result that transition would be expected to move forward on the model as time increased.

(iii) The presence of sound generated from the turbulent boundary layer on the tunnel walls[12] would be expected to disturb the boundary layer on the model and promote early transition at all times.

Of these (i) and (ii) are opposing effects, although (i) would die out quite rapidly with time. However it is probable that in fact (iii) is the dominant effect which tends to mask the others, and for the

purpose of calculating and classifying the heat-transfer results the transition position has therefore been considered to be fixed at the 4 inch station as indicated by the temperature distributions at each instant.

4.3. *Distributions of Heat Transfer.*

The distributions of heat transfer at various times obtained along the top generator of the model are shown in Fig. 9. In view of the errors in heat transfer due to accuracy of measurement of wall temperature, results for times greater than about 30 sec or so are of little value. (Section 3.2.3.)

Assuming transition position at $x = 4$ inches, where x is the distance along the surface from the tip, and starting from a particular level of heat transfer at transition, variations of heat transfer proportional to $x^{-1/2}$ and $x^{-1/5}$ are shown upstream and downstream of this point respectively by a dashed line. The former variation is appropriate to a laminar boundary layer and the latter (approximately) to a turbulent boundary layer when isothermal wall conditions apply. By scaling the dashed curve to the results at each given time, it appears that in the laminar region the variation of heat transfer with increasing distance from the tip is far more rapid than the inverse half power. In fact the inverse three-quarter power is more appropriate to the results. The turbulent results (i.e. beyond the 6 inch station) on the other hand behave as predicted and are not very sensitive to distance from the tip. Results, therefore, show very little longitudinal variation throughout the run.

4.3.1. *Laminar heat-transfer results.*—The laminar heat-transfer results obtained at stations within the first 4 inches of the cone tip are shown in Fig. 10. Here the results have been weighted by a factor of distance from the tip to the half power. As indicated earlier, although theoretical estimates from Refs. 10 and 11 would predict collapse of the results on this basis onto the single dashed line shown in the figure, some variation of the results with distance remains. Hence overall agreement of the experimental results with standard theoretical estimates is as a consequence only within 25%.

It should be noted that for these tests comparison of the experimental results with theoretical estimates on the basis of heat-transfer factors or Stanton numbers exhibit the same trends, since in the laminar region the wall temperature is fairly uniform at each instant and the recovery factors are virtually the same for each station.

Also shown in Fig. 10 is the result obtained at 5·06 inches from the tip, which from the classification made from the wall temperature distributions in Section 4.2 must be regarded as 'transitional'.

4.3.2. *Turbulent heat transfer.*—The turbulent heat-transfer results, obtained 6 inches or more from the cone tip, are shown in Fig. 11. As mentioned earlier the variation of heat transfer with distance from the tip was not large, and the distributions of heat transfer with time can be represented by two distinct curves labelled E and F in the figure. Of these the stations corresponding to curve E exhibit at each time a relatively higher heating rate than those corresponding to curve F. However, as can be seen from Fig. 8, the wall temperature at E-stations lies appreciably below that at F. It therefore follows that the heat transfer at the former stations would be expected to be correspondingly higher than the latter at each instant. The cause of this effective time-lag on the E heat-transfer results is probably due to thermal conduction aft to the Sindanyo plug supporting the base of the cone (see Fig. 1).

Because of the above discrepancy in the E-results, theoretical estimates of turbulent heat transfer based on Refs. 10 and 11 assuming the enthalpy recovery factor 0·88 found in Section 4.2, were

made only for the wall temperature-time variation appropriate to the F-family of curves. The calculations also assumed the boundary layer was fully turbulent from the tip and were performed for two positions along the cone surface. These are shown as dashed lines in Fig. 11. As can be seen the Reynolds number (or distance from the tip) effect is not large for these theoretical estimates, which appear to overestimate the results by as much as 50% when the region of very high % inaccuracy for the experimental results is approached. Agreement with experiment is much better however when higher heat-transfer rates are considered.

Appendix IV presents a calculation of the allowance which should be made on the theoretical estimates of heat transfer when an 'effective start' of the turbulent boundary layer upstream of transition is considered. The results from this calculation are illustrated in Fig. 12c and show that, for the present tests, the local heat transfer to the surface would be expected to be from 5 to 7% higher than the theoretical estimates shown in Fig. 11. The experimental results described therefore are that much more in general disagreement with theoretical results. Here again, as in the case of the results from the laminar region, little change in this picture emerges from basing the comparison with theory in terms of heat-transfer factors or Stanton numbers.

5. *Conclusions.*

Measurements of heat transfer on a 15° total-angle cone of graded wall thickness at zero incidence in the 6·8 airstream of the R.A.E. Hypersonic Tunnel gave the following results:

(1) The effect of grading wall thickness to maintain uniform wall temperatures throughout a run was reasonably successful, despite the fact that transition occurred on the model.

(2) The enthalpy recovery factor in the laminar region was predicted well by taking Prandtl number to the half power at intermediate enthalpy conditions[10, 11]. In the turbulent region the recovery factor found was 0·88. However, for both the experimental values found, since thermal-radiation effects were neglected, it is possible that they both underestimate true zero-heat-transfer conditions by an increment of up to 0·01 (*see* Appendix III).

(3) Heat transfer in the laminar region agreed with theoretical estimates from Refs. 10 and 11 to within 25%. The main trend of disagreement was that the experimental results varied something like an inverse $\frac{3}{4}$ power of distance back from the tip whereas theory and in fact the graded thickness of the model follow an inverse $\frac{1}{2}$ power.

(4) Heat transfer in the turbulent region was in good agreement with theoretical estimates from Refs. 10 and 11 during the period of high heat transfer early in the run. However, as the run proceeded, although the accuracy of the results themselves deteriorated with time, their agreement with the theoretical values deteriorated even faster, and during the period of low heat-transfer rates, theoretical results appeared to overestimate them by about 50%.

LIST OF SYMBOLS

M	Mach number
M_∞	Free-stream Mach number
M_c	Mach number at the edge of the boundary layer along the cone surface
T	Temperature in °K (except where otherwise stated)
T_w	Wall temperature
T_0	Stagnation or total temperature
T_r	Recovery temperature
T_1	Ambient temperature at the edge of the boundary layer along the cone surface
T_i	Wall temperature at $t = 0$
T^*	Intermediate temperature corresponding to $i^*(r)$
t	Time in seconds
i	Enthalpy in $\frac{\text{C.H.U.}}{\text{lb}}$
i_0	Stagnation or total enthalpy $\left(= i_1 + \frac{{u_1}^2}{2gJ}\right)$
i_r	Recovery enthalpy $\left(= i_1 + \frac{r{u_1}^2}{2gJ}\right)$
i_1	Ambient enthalpy at the edge of the boundary layer along the cone surface
$i^*(r)$	Intermediate enthalpy defined in Appendix IV
r	Enthalpy recovery factor $\left(= \frac{i_r - i_1}{i_0 - i_1}\right)$
J	Mechanical equivalent of heat $\left(\frac{\text{ft lb}}{\text{C.H.U.}}\right)$
u_1	Velocity at the edge of the boundary layer (ft/sec)
u	Velocity in the boundary layer (ft/sec)
ρ	Density in the boundary layer $\left(\frac{\text{slugs}}{\text{ft}^3}\right)$
ρ_1	Density at the edge of the boundary layer $\left(\frac{\text{slugs}}{\text{ft}^3}\right)$
ρ_I	Density of air inside model $\left(\frac{\text{slugs}}{\text{ft}^3}\right)$
$\rho(T)$	Density of the nickel skin $\left(\frac{\text{lb}}{\text{ft}^3}\right)$

LIST OF SYMBOLS—*continued*

c_p	Specific heat of air at constant pressure $\left(\frac{\text{C.H.U.}}{\text{slug °K}}\right)$
$c(T)$	Specific heat of the nickel skin $\left(\frac{\text{C.H.U.}}{\text{lb °K}}\right)$
α	Thermal diffusivity $\left(\frac{\text{ft}^2}{\text{sec}}\right)$
$k(T)$	Thermal conductivity of nickel skin $\left(\frac{\text{C.H.U.}}{\text{ft sec °K}}\right)$
μ_1	Viscosity of air at temperature T_1 $\left(\frac{\text{lb}}{\text{ft sec}}\right)$
μ^*	Viscosity of air at temperature T^* $\left(\frac{\text{lb}}{\text{ft sec}}\right)$
s	Distance from nose of cone along a generator in feet
x	Distance from leading edge on a flat plate, distance from tip on a cone. (In ft except where otherwise stated.)
x_T	Position of transition along model surface. (In ft except where otherwise stated.)
x_0	Position of 'effective start' of the turbulent boundary layer. (In ft except where otherwise stated.)
y	Distance perpendicular to the wall through boundary layer
δ	Boundary-layer thickness
θ	Momentum thickness of boundary layer $\left(= \int_0^\delta \left(1 - \frac{u}{u_1}\right) \frac{\rho u}{\rho_1 u_1} dy\right)$
$d(s)$	Skin thickness in feet
Re/ft	Reynolds number per foot
R_x	Reynolds number based on x at conditions at the edge of the boundary layer $\left(= \frac{\rho_1 u_1 x}{\mu_1}\right)$
τ_w	Surface shear (lb/ft²)
c_f	Local skin-friction coefficient $\left(= \frac{\tau_w}{\frac{1}{2}\rho_1 {u_1}^2}\right)$
p_c	Pressure on cone
p_0	Tunnel stagnation pressure
V_I	Volume of air inside model (ft³)
$H(t)$	Heat content of air inside model (C.H.U.)

LIST OF SYMBOLS—*continued*

A_w	Radiating area for model (ft^2)
A_s	Radiating area for surroundings (ft^2)
ϵ_w	Emissivity of wall
ϵ_s	Emissivity of surroundings
$h(s,\ T_w)$	Heat-transfer factor $\left(\frac{\text{C.H.U.}}{\text{ft}^2\ \text{sec}\ ^\circ\text{K}}\right)$
$H(T_w)$	Function of T_w defined in equation (2) Appendix I $\left(\frac{\text{C.H.U.}}{\text{ft}^{3/2}\ \text{sec}\ ^\circ\text{K}}\right)$
$\dot{q}''$	Aerodynamic heating to surface of model $\left(\frac{\text{C.H.U.}}{\text{ft}^2\ \text{sec}}\right)$
$\dot{q}''_{\text{T.S.}}$	Thin skin approximation to $\dot{q}''$ defined by equation (3) Appendix I $\left(\frac{\text{C.H.U.}}{\text{ft}^2\ \text{sec}}\right)$
$\dot{q}''_c$	Heat transferred by thermal conduction $\left(\frac{\text{C.H.U.}}{\text{ft}^2\ \text{sec}}\right)$
$\dot{q}''_R$	Resultant heat transmitted by thermal radiation from walls of model $\left(\frac{\text{C.H.U.}}{\text{ft}^2\ \text{sec}}\right)$
$\dot{q}''_I$	Heat loss to inside of model $\left(\frac{\text{C.H.U.}}{\text{ft}^2\ \text{sec}}\right)$
τ	Time constant for exponential surface temperature rise on the model (sec)

REFERENCES

No.	*Author(s)*	*Title, etc.*
1	L. F. Crabtree and J. F. W. Crane	The 7 in. × 7 in. Hypersonic Wind Tunnel at R.A.E. Farnborough. Part I. Design, instrumentation and flow visualization techniques. A.R.C. C.P. 590. August, 1961.
2	J. F. W. Crane	The 7 in. × 7 in. Hypersonic Wind Tunnel at R.A.E. Farnborough. Part II. Heater performance. A.R.C. C.P. 590. August, 1961.
3	J. F. W. Crane	The 7 in. × 7 in. Hypersonic Wind Tunnel at R.A.E. Farnborough. Part III. Calibration of the flow in the working section. A.R.C. C.P. 590. August, 1961.
4	Consolidated Electrodynamics Corporation.	Type 37–103/electromanometer. Operation and maintenance manual. C.E.C. 300 North Sierra, Madre Villa, Pasadena, California, U.S.A.
5	Honeywell Controls Limited ..	Type 153 quarter-second electronik recorder. Instruction manual. Honeywell-Brown Ltd., 1, Wadsworth Road, Perivale, Greenford, Middlesex.
6	J. G. Woodley	Pressure measurements on a cone-cylinder-flare configuration at small incidences for $M = 6{\cdot}8$. A.R.C. C.P. 632. March, 1961.
7	Leeds & Northrup Company ..	Speedomax Type G recorders. Models 60,000 series. Philadelphia 44, U.S.A.
8	J. E. Couper	The operation and maintenance of recorder Type IT 3-13-61. Unpublished M.o.A. Report.
9	Z. Kopal (Ed.)	Tables of supersonic flow around yawing cones. M.I.T. Center of Analysis Technical Report No. 3. 1947.
10	R. J. Monaghan	Formulae and approximations for aerodynamic heating rates in high speed flight. A.R.C. C.P. 360. October, 1955.
11	L. F. Crabtree and J. G. Woodley	Skin friction drag and aerodynamic heating. *Handbook of supersonic aerodynamic data.* Vol. 2, Chapter 8. November, 1959.
12	J. Laufer	Aerodynamic noise in supersonic wind tunnels. *J. Aero./Space Sci.*, Vol. 28, No. 9. September, 1961.

APPENDIX I

Design of Graded-Thickness Cone Model

Convective heat transfer, $\dot{q}''$, to a cone of surface temperature T_w at a position distance s from the nose along a generator, is given by:

$$\dot{q}'' = h(s,\ T_w)(T_r - T_w) \tag{1}$$

where T_r is the recovery temperature, and $h(s,\ T_w)$ the heat-transfer factor.

For a laminar boundary layer with the cone at zero incidence to the airstream $h(s,\ T_w)$ is inversely proportional to the square root of s. Thus in this case:

$$h(s,\ T_w) = H(T_w)s^{-1/2}. \tag{2}$$

If $d(s)$ is the thickness of the skin at this position, then, if the skin is assumed to be thermally-thin, we can also relate the convective heat transfer to the rate of rise of wall temperature. Hence:

$$\dot{q}'' = \rho(T_w)c(T_w)d(s)\frac{\partial T_w}{\partial t} \tag{3}$$

where $\rho(T_w)$ is the density and $c(T_w)$ is the specific heat of the skin material.

From equations (1), (2) and (3) we obtain:

$$\frac{\partial T_w}{\partial t} = \frac{H(T_w)}{\rho(T_w)c(T_w)}[d(s)s^{1/2}]^{-1}(T_r - T_w). \tag{4}$$

Thus it follows that if the skin thickness is made such that $d(s)s^{1/2}$ is a constant (K), equation (4) becomes independent of position and all points on the cone, being isothermal at the start of a run, should warm up uniformly in the airstream, provided only that laminar conditions prevail. Longitudinal conduction effects are therefore theoretically eliminated by this technique.

In particular since $H(T_w)/\rho(T_w)c(T_w)$ in general varies slowly with T_w, equation (4) in fact can be written:

$$\frac{dT_w}{dt} = \frac{H(T_i)}{\rho(T_i)c(T_i)K}(T_r - T_w) \tag{5}$$

where T_i is the initial wall temperature.

This has the solution:

$$\frac{(T_r - T_w)}{(T_r - T_i)} = e^{-t/\tau} \tag{6}$$

where τ is the time constant and equals $\rho(T_i)c(T_i)K/H(T_i)$. In the present tests τ was taken (by suitable choice of K *via* skin thickness) to be of the order of 10 seconds. This allowed for the complete range of wall temperature from T_i to T_r to be covered in 30 sec or so of a run.

Check that Designed Model Skin was Thermally-Thin.

Consider the case of one-dimenstional heat flow in a slab of material of thickness d and constant thermal diffusivity α, with heat applied to its outer surface and an insulated inner surface. If we assume that at any instant the temperature profile through the slab can be represented by an infinite

power series in distance from the inner surface, with coefficients functions of time. Then it follows that the temperature at the outer surface, T_{outer}, and the temperature at the inner surface, T_{inner}, are connected by the relation:

$$T_{\text{outer}} = T_{\text{inner}} + \sum_{n=1}^{\infty} \frac{1}{(2n)!} \left(\frac{d^2}{\alpha}\right)^n \frac{d^n T_{\text{inner}}}{dt^n}. \tag{7}$$

For the present model this relation, applied to the results at the station where the skin was thickest, gave a maximum temperature difference across the skin of the order of $\frac{1}{5}$°C.

APPENDIX II

The Electromanometer System Used in the Hypersonic Tunnel at R.A.E., Farnborough

One of the instruments used for measuring pressures in the R.A.E. Hypersonic Tunnel[1] is the Electromanometer Type 37-103[4], which is manufactured by the Consolidated Engineering Corporation, Pasadena, California. This employs a servo system which produces a null balance between two pressure-sensitive bellows, one of which contains a reference pressure and is separated by a diaphragm from the other bellows which is fed with the pressure to be measured. Two pressure heads are available, one for the range up to 1·5 p.s.i. and the other up to 15 p.s.i. Visual read-out is by means of a Honeywell Brown Electronik high-speed-strip chart recorder[5], which has a full-scale balancing time of $\frac{1}{4}$ sec. The electrical output from the manometer will eventually be fed directly to the analogue to digital converter of a data-logging system which is available for general measurements in the tunnel.

Electromanometer System.

A block diagram of the electromanometer system used for measuring surface pressures on a model is shown in Fig. 4. In this diagram the part of the system used to record the surface pressure is shown outside the dashed rectangle. To save duplication of the equipment a Scanivalve (rotary pressure switch made by General Design Co., San Diego, California) is used, and during a test pressures are individually selected and recorded. The low reference pressure on one side of the transducer is supplied by a vacuum pump and it is measured by a McLeod gauge. A by-pass valve is used across the transducer in order that the pressures in the bellows can easily be equalised to avoid overload and possible damage from atmospheric leaks when the 1·5 p.s.i. head is used. This is important since the head can stand only 25% overload without permanent damage.

The part of the system shown inside the dashed rectangle is used to calibrate the transducer, and the method of doing this using a C.E.C. Type 6-201 Primary Pressure Standard (dead-weight tester) is given in Ref. 6.

APPENDIX III

Effect on Heat-Transfer Results of Conduction in the Skin, Thermal Radiation from the Walls, and Heat Loss to the Interior of the Model

In the notation of Appendix I, the heat-balance equation (3) on an element of a thermally-thin skin, when conduction and other thermal effects are significant, must be written:

$$\dot{q}'' = \dot{q}''_{\text{T.S.}} - \dot{q}''_c + \dot{q}''_R + \dot{q}''_I \tag{8}$$

where, per unit surface area per unit time:

$\dot{q}''$ is the convective heat transfer

$$\dot{q}''_{\text{T.S.}} \left(= \rho(T_w)c(T_w)d(s)\frac{\partial T_w}{\partial t} \right)$$

is the standard thin-skin approximation to $\dot{q}''$, since it represents the rate at which heat is accumulated in the skin.

$\dot{q}''_c$ is the heat transferred by conduction,

$\dot{q}''_R$ is the resultant heat transmitted by thermal radiation from the walls,

$\dot{q}''_I$ is the heat lost by conduction, radiation and free convection to the air inside the model.

For the present tests all but the first term in equation (8) were neglected, and the results were calculated by equation (3). The effects of this on the accuracy of the results are considered below.

(i) *Effect of Neglecting* $\dot{q}''_c$.

From consideration of an element of the wall of the cone we see that:

$$\dot{q}''_c(s, t) = \frac{1}{s}\frac{\partial}{\partial s}\left[sd(s)k(T_w)\frac{\partial T_w}{\partial s} \right] \tag{9}$$

where $k(T_w)$ is the thermal conductivity of the skin at temperature T_w. Since $d(s)$, the wall thickness, varies as $s^{-1/2}$, equation (9) reduces to:

$$\dot{q}''_c = k(T_w)d(s)\left\{ \frac{1}{2s}\frac{\partial T_w}{\partial s} + \frac{\partial^2 T_w}{\partial s^2} \right\} \tag{10}$$

if the thermal conductivity of the wall is assumed constant at the wall temperature level considered.

In the present analysis of the tests only rough calculation of $\dot{q}''_c$ from the temperature distributions along the cone was possible, and this indicated that at some stations the effect of the heat-conduction term could at times have been of the order of 10% of $\dot{q}''_{\text{T.S.}}$. It was not possible, however, to systematically allow for this effect in the results.

(ii) *Effect of Neglecting* $\dot{q}''_R$.

Inside the model losses from thermal radiation should be small, since near radiation-equilibrium might be expected. However, such losses as do in fact occur must be included in $\dot{q}''_I$, which will later be shown to be insignificant anyway.

In view of this, we have that for the loss of heat from the outside of the model:

$$\dot{q}''_R \simeq \frac{2{\cdot}78\ 10^{-12}}{\left[\frac{1}{\epsilon_w} + \left(\frac{A_w}{A_s}\right)\left(\frac{1}{\epsilon_s} - 1\right)\right]} [T_w{}^4 - T_s{}^4] \left(\frac{\text{C.H.U.}}{\text{ft}^2\ \text{sec}}\right)$$

where A_w, ϵ_w and T_w(°K) are respectively the radiating area, emissivity, and wall temperature of the model, and A_s, ϵ_s and T_s 'appropriate' parameters for its surroundings.

A maximum value for $\dot{q}''_R$ would correspond to the case when the surroundings behaved as a black body with $\epsilon_s = 1$, and in any case this is the solution appropriate to A_w/A_s small.

In either case therefore we have:

$$(\dot{q}''_R)_{\max} \simeq 2{\cdot}78\epsilon_w \left[\left(\frac{T_w}{10^3}\right)^4 - \left(\frac{T_s}{10^3}\right)^4\right] \left(\frac{\text{C.H.U.}}{\text{ft}^2\ \text{sec}}\right).$$

Since, over the range of temperatures considered for the nickel model, $\epsilon_w \simeq 0{\cdot}12\ (T_w/10^3)$ and in general T_s will be somewhat less than T_w, a conservative estimate is:

$$(\dot{q}''_R)_{\max} \simeq \frac{1}{3}\left(\frac{T_w}{10^3}\right)^5 \left(\frac{\text{C.H.U.}}{\text{ft}^2\ \text{sec}}\right).$$

This formula gives approximately 0·03 (C.H.U./ft² sec) at the temperature reached by the model at a time 60 seconds from the start of the run. As can be seen from Fig. 9, this is a significant part of the total heat transfer at this time. However, since the % inaccuracy of the heat-transfer values derived from temperature-time profiles is large after 20 to 30 seconds from the start of a run (Section 3.2.3), this effect of radiation is appreciable only when the results are of little importance anyway. It is of note that the decrease in the true recovery temperature the thermal radiation term would introduce is equal to $\dot{q}''_R/h(T_w)$, where $h(T_w)$ is the heat-transfer factor based on the temperature at the station considered. At 60 seconds from the start of the run this difference between real and measured recovery temperatures has a maximum value of about 6°K, which means that the measured enthalpy recovery factor at this time can be as much as 0·01 below the true value.

(iii) *Effect of Neglecting* $\dot{q}''_I$.

Within the conical model a very conservative limit on the thermal energy, $\dot{q}''_I$, which could be transmitted to the air at each instant by the various mechanisms, would be that which would be required to maintain the air at the same temperature as the wall.

Since the thin conical shell of the model contained a few small holes, it is reasonable to assume that the air pressure inside the model was maintained at the static pressure existing on the cone surface.

Thus, if $H(t)$ is the total heat contained in the air within the model at time t, using the above assumptions:

$$H(t) = \rho_I V_I(c_p T_w) = c_p V_I(\rho_I T_w),$$

where c_p, the specific heat of air at constant pressure, is assumed constant, and ρ_I and V_I are the density and volume of the internal air.

But by the equation of state for air $p \propto \rho T$ and the fact that inside the cone the static pressure p_c is maintained, we have:

$$H(t) \propto c_p p_c V_I = \text{constant}.$$

Thus under the assumptions made the total heat contained in the air inside the model is a constant, $H(0)$, and the heat added at any instant is balanced by the heat lost with the air which expands through the vents into the main airstream. Therefore in time Δt, if the wall temperature is increased by ΔT_w:

$$\dot{q}''_I \Delta t\, A = \text{Heat added to the air inside the model}$$

$$= H(0)\left(\frac{T_w + \Delta T_w}{T_w}\right) - H(0)$$

$$= H(0)\frac{\Delta T_w}{T_w},$$

where

A = Area through which this heat is transmitted.

Hence

$$\dot{q}''_I = \frac{H(0)}{A}\frac{1}{T_w}\frac{dT_w}{dt}. \tag{11}$$

In the present tests $H(0)/A \simeq 8{\cdot}3 \times 10^{-3}$(C.H.U./ft²), and this gives that $\dot{q}''_I \simeq 2 \times 10^{-3}$(C.H.U./ft² sec) for the worst possible case in the results. This effect can therefore be completely neglected.

APPENDIX IV

Effective Start of the Turbulent Boundary Layer on the Cone as a Function of Transition Reynolds Number and Wall Temperature

For both fully laminar and fully turbulent flow we can take the following steps:

(i) Assume local incompressible skin-friction coefficient on a flat plate, $(c_{fi})_{\text{f.p.}}$, as a function of the local Reynolds number, R_x, based on distance, x, from the leading edge, in the form:

$$(c_{fi})_{\text{f.p.}} = \alpha R_x^{\beta},$$

where α and β are constants.

(ii) Apply intermediate enthalpy method[10, 11] to obtain compressible skin-friction coefficient on a flat plate, $(c_f)_{\text{f.p.}}$, in form:

$$(c_f)_{\text{f.p.}} = \alpha^* R_x^{\beta},$$

with

$$\alpha^* = \alpha \left(\frac{T_1}{T^*}\right)^{\beta+1} \left(\frac{\mu_1}{\mu^*}\right)^{\beta},$$

where μ and T are respectively temperature and viscosity, and suffix 1 denotes local free-stream conditions. The starred conditions correspond to evaluation at a temperature T^* which corresponds to an intermediate enthalpy $i^*(r)$ derived from the formula:

$$\frac{i^*(r)}{i_1} = 1 + 0{\cdot}5\left(\frac{i_w}{i_1} - 1\right) + 0{\cdot}044 r M_e^2,$$

where M_e is local Mach number, r is an appropriate enthalpy recovery factor, and suffix w denotes conditions at the wall.

(iii) Use a shape factor[11] to relate $(c_f)_{\text{f.p.}}$ to local skin-friction coefficient on a cone, $(c_f)_{\text{cone}}$.

$$\frac{(c_f)_{\text{cone}}}{(c_f)_{\text{f.p.}}} = \gamma,$$

where γ is a constant.

(iv) Substitute $(c_f)_{\text{cone}}$ into the integral momentum equation for a cone.

$$\tfrac{1}{2}(c_f)_{\text{cone}} = \frac{d\theta}{dx} + \frac{\theta}{x} = \frac{1}{x}\frac{d(x\theta)}{dx},$$

where θ is the momentum thickness.

Integration then gives:

$$R_\theta = \gamma^* R_x^{(\beta+1)},$$

where

$$\gamma^* = \frac{\gamma\alpha^*}{2(\beta+2)}. \tag{12}$$

The various parameters used in (i) to (iv) above are:

Parameter	Laminar	Turbulent
α	0·664	0·0592
β	$-\frac{1}{2}$	$-\frac{1}{5}$
γ	$\sqrt{3}$	1·15
r	$(Pr^*)^{1/2}$, used in Fig. 7, where Pr is Prandtl No.	0·89
M_c	5·88 (*See* Section 4.1)	

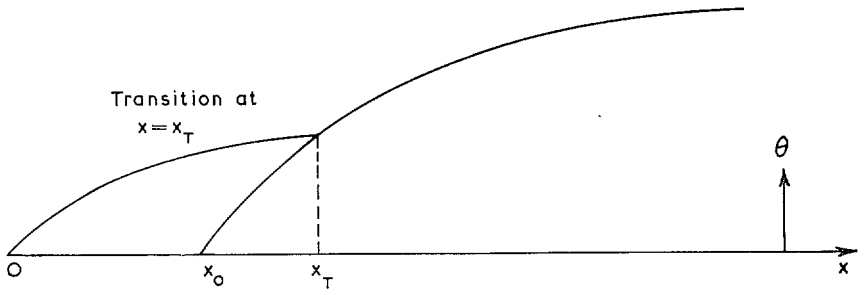

If we now assume that on the cone the momentum thickness is continuous at transition as illustrated in the above sketch, then we may imagine the 'effective start' of the turbulent boundary layer to be at a point $x = x_0$, and by matching the momentum thickness, θ_T, at the transition point, $x = x_T$, using (12) applied to the laminar and turbulent regions we obtain:

$$\frac{R_{(x_T-x_0)}}{(R_{x_T})^{5/8}} = \frac{(R_{x_T}-R_{x_0})}{(R_{x_T})^{5/8}} = 43\,\frac{\left\{\left(\frac{T_1}{T^*}\right)^{5/8}\left(\frac{\mu_1}{\mu^*}\right)^{-5/8}\right\}_{r\text{ laminar value}}}{\left\{\left(\frac{T_1}{T^*}\right)\left(\frac{\mu_1}{\mu^*}\right)^{-1/4}\right\}_{r\text{ turbulent value}}} \tag{13}$$

together with:

$$\frac{R_{\theta_T}}{(R_{x_T})^{1/2}} = 0{\cdot}3873\left\{\left(\frac{T_1}{T^*}\right)^{1/2}\left(\frac{\mu^*}{\mu_1}\right)^{1/2}\right\}_{r\text{ laminar value}}. \tag{14}$$

For the conditions and range of wall temperature in the present tests, equations (13) and (14) have been illustrated in Figs. 12a and 12b respectively. As can be seen from Figs. 3 and 12b, with $x_T = 4$ inches (considered in Section 4.2) we have that for most of the run $R_{x_T} \simeq 2{\cdot}8 \times 10^6$ and $R_{\theta_T} \simeq 585$. The value of R_{x_0} will correspondingly vary therefore throughout a run, using Fig. 12a, from about $1{\cdot}6 \times 10^6$ to $1{\cdot}25 \times 10^6$, which means that x_0 will vary from about 2·3 to 1·8 inches from the tip.

Fig. 12c shows the effect that the allowance for $x_0 \neq 0$ will have on the theoretical estimates of heat transfer given in Fig. 11 at two positions along the cone. In general this amounts to an increase of from 5 to 7% on the heat-transfer values used for comparison with the results in Fig. 11.

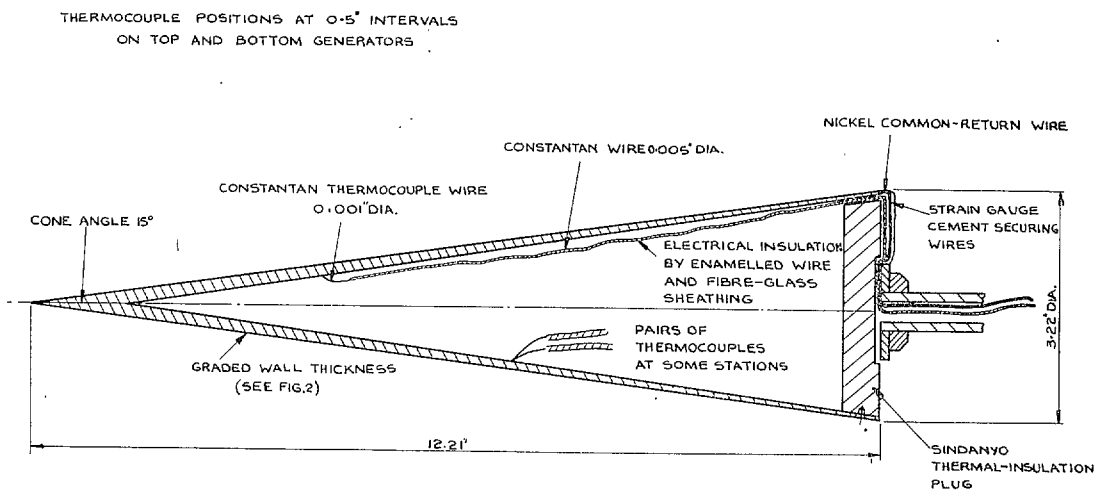

FIG. 1. Thin-wall nickel cone (not to scale).

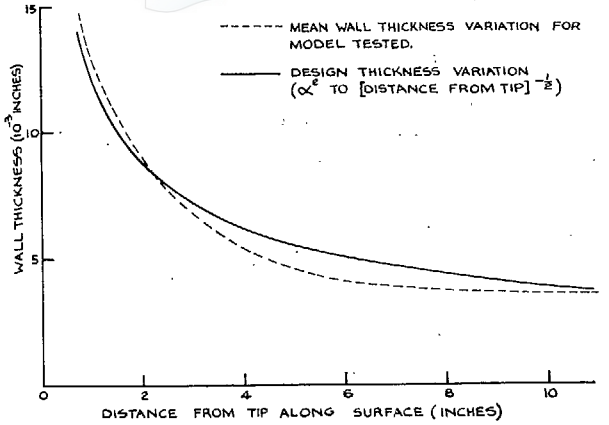

(a) WALL THICKNESS VARIATION WITH DISTANCE.

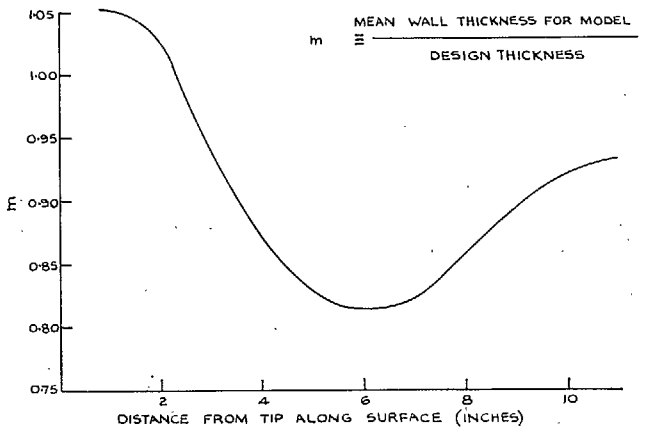

(b) VARIATION OF PARAMETER m WITH DISTANCE.

FIG. 2. Wall thickness variation of cone model.

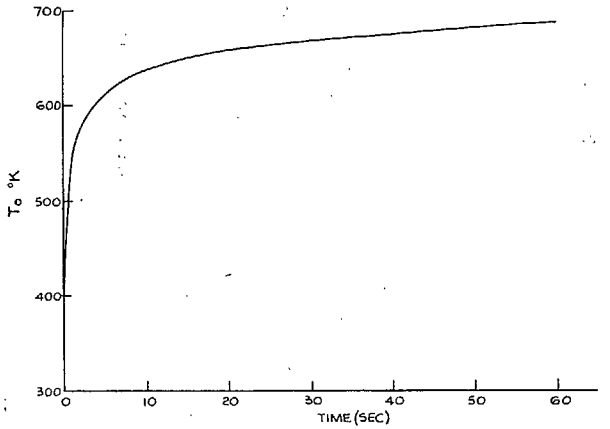

(a) STAGNATION TEMPERATURE (T_0) VS. RUNNING TIME.

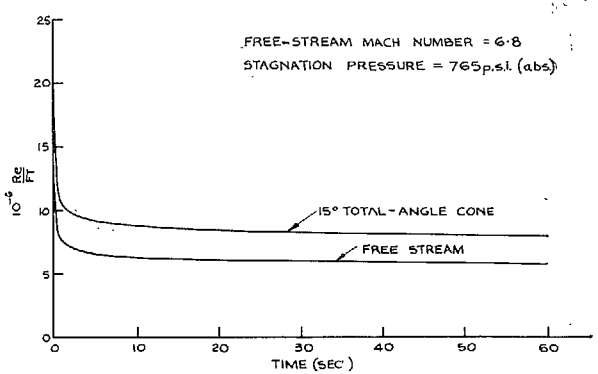

(b) REYNOLDS NUMBER PER FOOT FOR CONDITIONS ON THE CONE AND IN THE FREE STREAM VS. RUNNING TIME.

FIG. 3. Test conditions at $M_\infty = 6{\cdot}8$ in the 7 in. × 7 in. Hypersonic Tunnel.

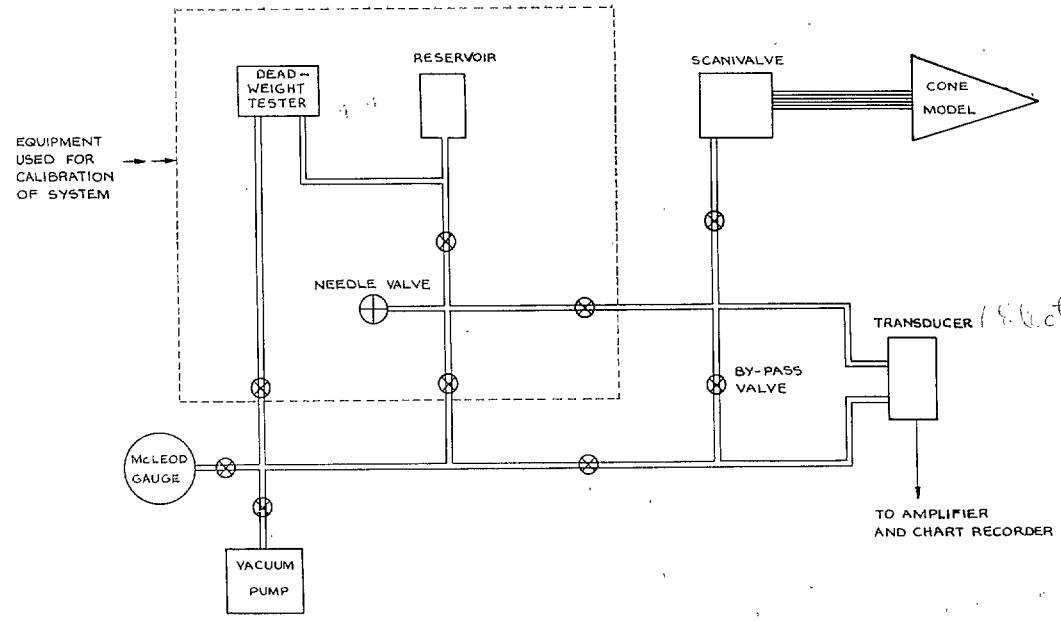

FIG. 4. The electromanometer system.

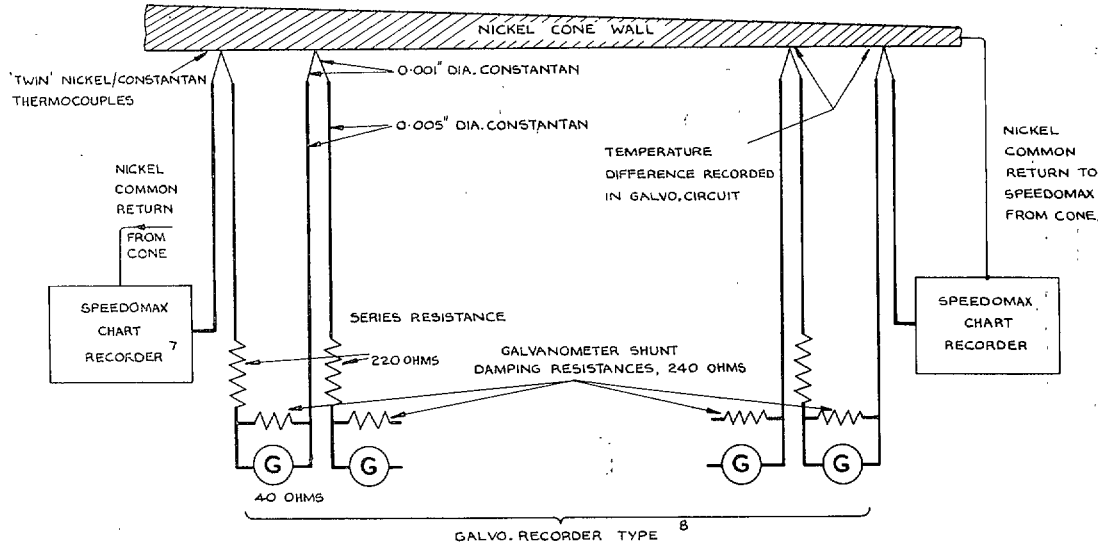

FIG. 5. Method of measuring skin temperatures by means of 'twin' thermocouples and galvanometer recorders, using Speedomax (potentiometer) recorders as a means of obtaining absolute-temperature reference.

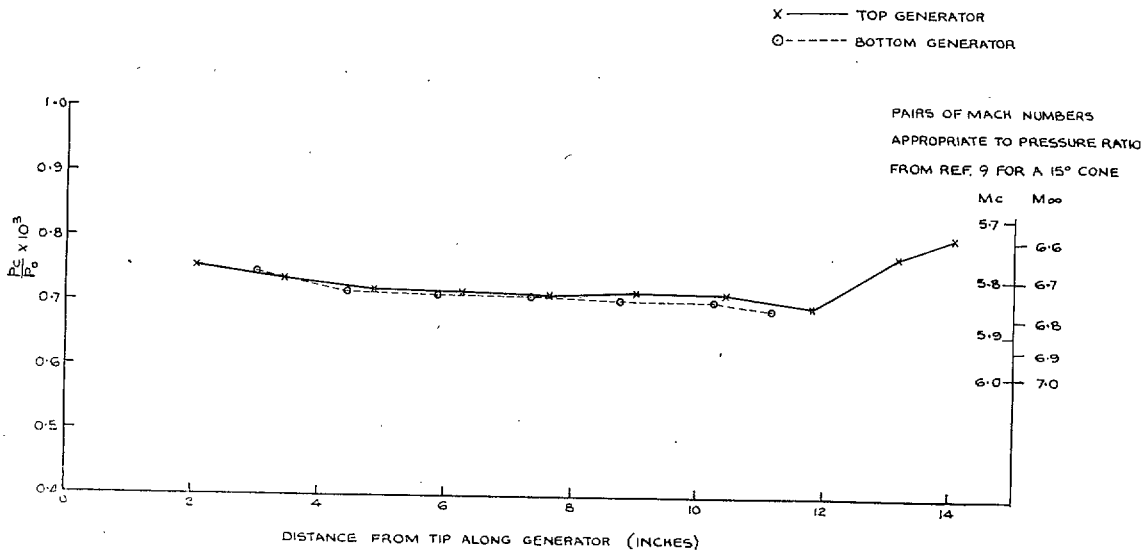

FIG. 6. Pressure distributions on the top and bottom generators of the pressure model at zero incidence.

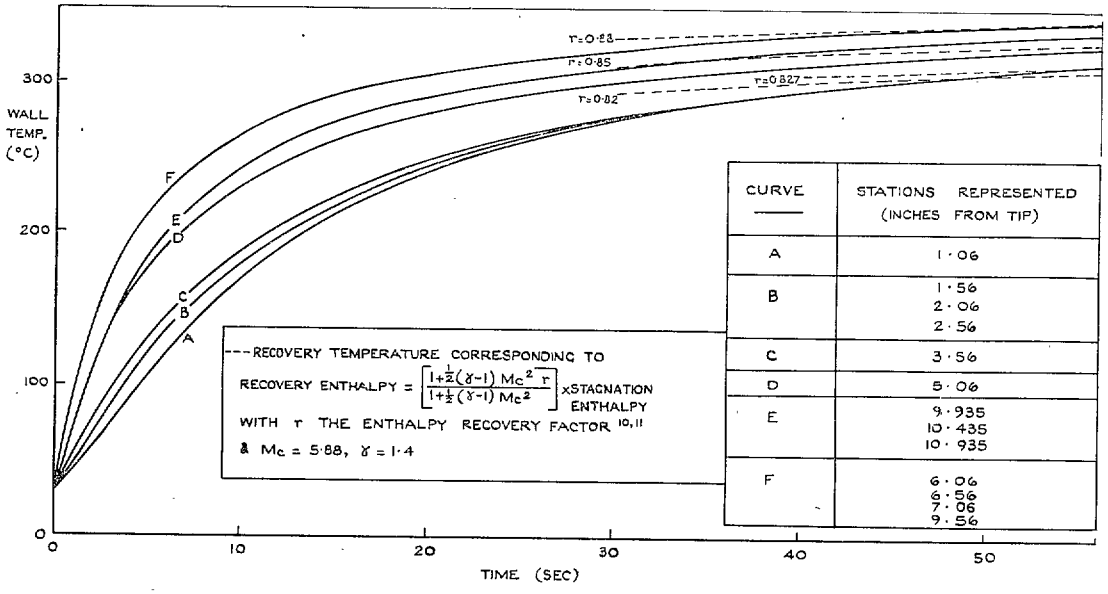

FIG. 7. Temperature-time histories at various representative stations along the top generator of the cone (zero incidence).

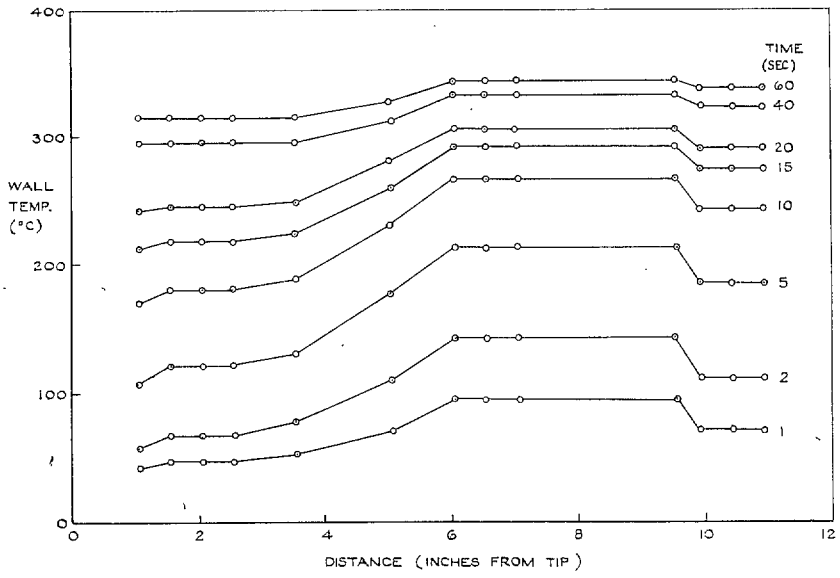

FIG. 8. Distribution of wall temperature at various times on the top generator of the cone.

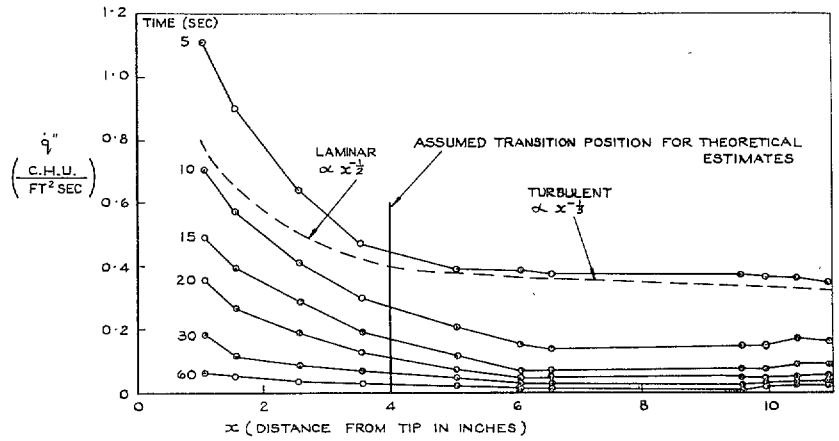

FIG. 9. Heat transfer along the top generator of the cone at various times (zero incidence).

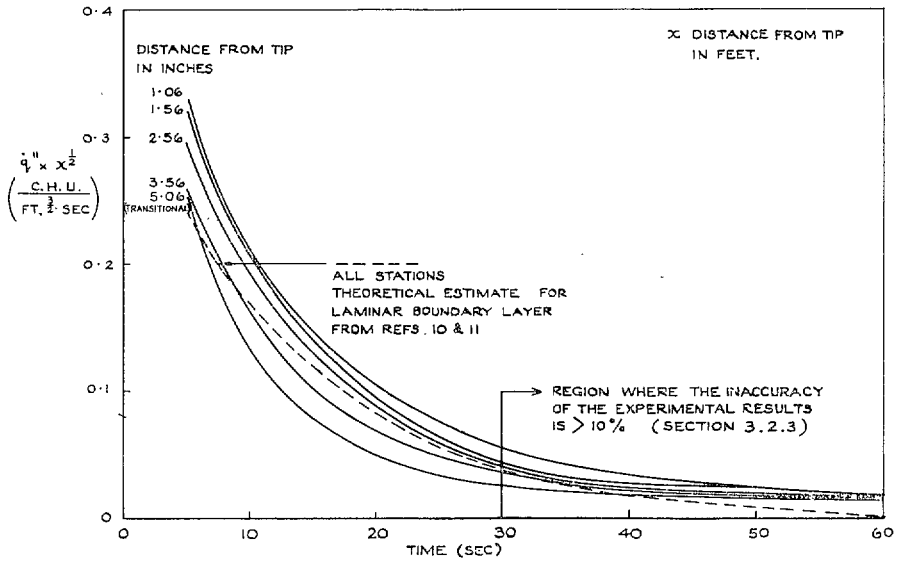

FIG. 10. Laminar heat-transfer results on the top generator of the cone.

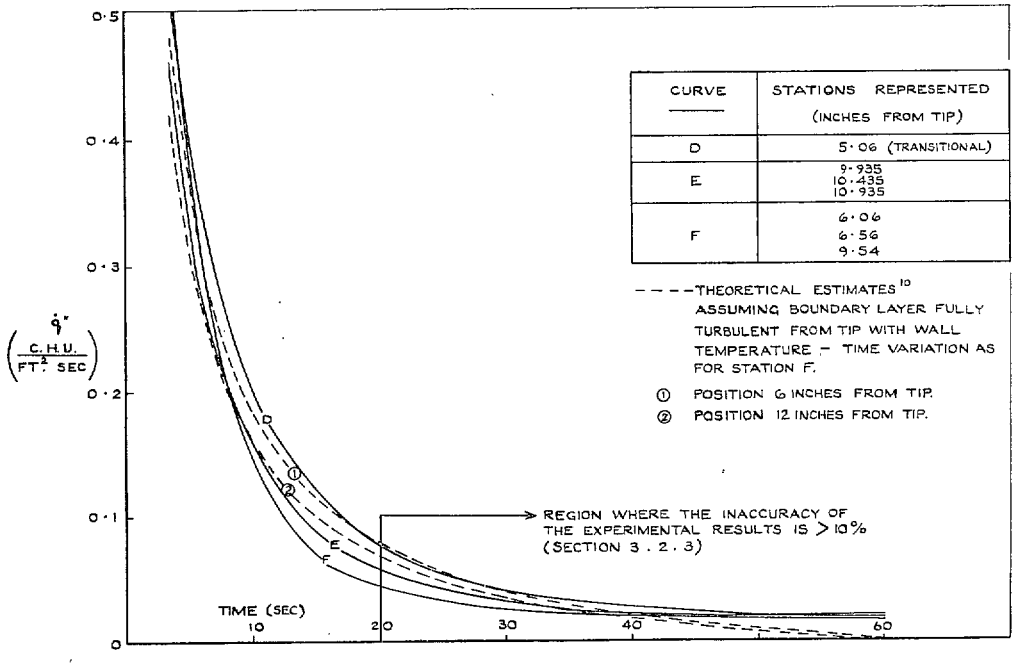

FIG. 11. Turbulent heat-transfer results on the top generator of the cone.

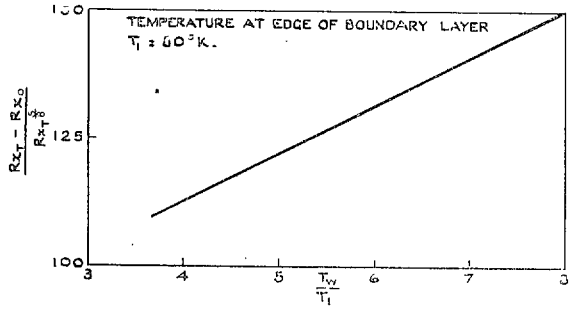

(a) DEPENDENCE OF EFFECTIVE START OF TURBULENT BOUNDARY LAYER, x_0, ON WALL TEMPERATURE, T_W, AND TRANSITION POSITION, x_T.

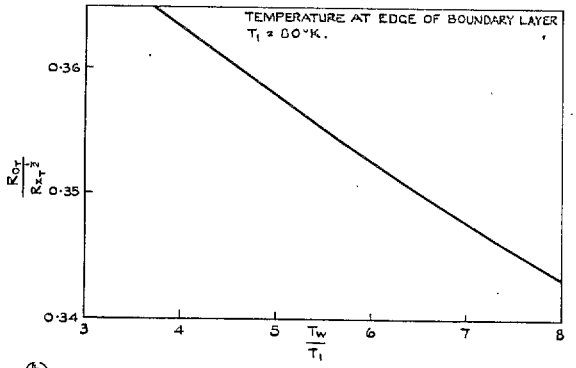

(b) MOMENTUM THICKNESS AT TRANSITION, θ_T, IN TERMS OF WALL TEMPERATURE, T_W, AND TRANSITION POSITION, x_T.

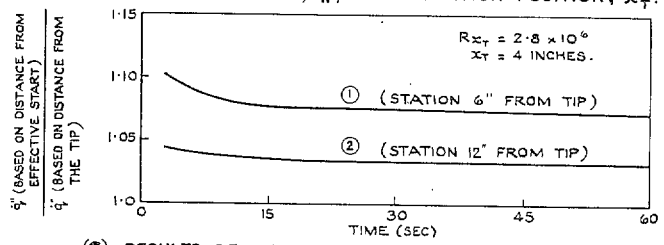

(c) RESULTS OF ALLOWING FOR EFFECTIVE START OF TURBULENT BOUNDARY LAYER IN THE ESTIMATES OF FIG. 11.

FIG. 12. Effect of transition on turbulent heat transfer.

(88724) Wt. 65/1418 K.5 2/64 Hw.

Publications of the Aeronautical Research Council

ANNUAL TECHNICAL REPORTS OF THE AERONAUTICAL RESEARCH COUNCIL (BOUND VOLUMES)

1942 Vol. I. Aero and Hydrodynamics, Aerofoils, Airscrews, Engines. 75*s.* (post 2*s.* 9*d.*)
Vol. II. Noise, Parachutes, Stability and Control, Structures, Vibration, Wind Tunnels. 47*s.* 6*d.* (post 2*s.* 3*d.*)

1943 Vol. I. Aerodynamics, Aerofoils, Airscrews. 80*s.* (post 2*s.* 6*d.*)
Vol. II. Engines, Flutter, Materials, Parachutes, Performance, Stability and Control, Structures. 90*s.* (post 2*s.* 9*d.*)

1944 Vol. I. Aero and Hydrodynamics, Aerofoils, Aircraft, Airscrews, Controls. 84*s.* (post 3*s.*)
Vol. II. Flutter and Vibration, Materials, Miscellaneous, Navigation, Parachutes, Performance, Plates and Panels, Stability, Structures, Test Equipment, Wind Tunnels. 84*s.* (post 3*s.*)

1945 Vol. I. Aero and Hydrodynamics, Aerofoils. 130*s.* (post 3*s.* 6*d.*)
Vol. II. Aircraft, Airscrews, Controls. 130*s.* (post 3*s.* 6*d.*)
Vol. III. Flutter and Vibration, Instruments, Miscellaneous, Parachutes, Plates and Panels, Propulsion. 130*s.* (post 3*s.* 3*d.*)
Vol. IV. Stability, Structures, Wind Tunnels, Wind Tunnel Technique. 130*s.* (post 3*s.* 3*d.*)

1946 Vol. I. Accidents, Aerodynamics, Aerofoils and Hydrofoils. 168*s.* (post 3*s.* 9*d.*)
Vol. II. Airscrews, Cabin Cooling, Chemical Hazards, Controls, Flames, Flutter, Helicopters, Instruments and Instrumentation, Interference, Jets, Miscellaneous, Parachutes. 168*s.* (post 3*s.* 3*d.*)
Vol. III. Performance, Propulsion, Seaplanes, Stability, Structures, Wind Tunnels. 168*s.* (post 3*s.* 6*d.*)

1947 Vol. I. Aerodynamics, Aerofoils, Aircraft. 168*s.* (post 3*s.* 9*d.*)
Vol. II. Airscrews and Rotors, Controls, Flutter, Materials, Miscellaneous, Parachutes, Propulsion, Seaplanes, Stability, Structures, Take-off and Landing. 168*s.* (post 3*s.* 9*d.*)

1948 Vol. I. Aerodynamics, Aerofoils, Aircraft, Airscrews, Controls, Flutter and Vibration, Helicopters, Instruments, Propulsion, Seaplane, Stability, Structures, Wind Tunnels. 130*s.* (post 3*s.* 3*d.*)
Vol. II. Aerodynamics, Aerofoils, Aircraft, Airscrews, Controls, Flutter and Vibration, Helicopters, Instruments, Propulsion, Seaplane, Stability, Structures, Wind Tunnels. 110*s.* (post 3*s.* 3*d.*)

Special Volumes

Vol. I. Aero and Hydrodynamics, Aerofoils, Controls, Flutter, Kites, Parachutes, Performance, Propulsion, Stability. 126*s.* (post 3*s.*)
Vol. II. Aero and Hydrodynamics, Aerofoils, Airscrews, Controls, Flutter, Materials, Miscellaneous, Parachutes, Propulsion, Stability, Structures. 147*s.* (post 3*s.*)
Vol. III. Aero and Hydrodynamics, Aerofoils, Airscrews, Controls, Flutter, Kites, Miscellaneous, Parachutes, Propulsion, Seaplanes, Stability, Structures, Test Equipment. 189*s.* (post 3*s.* 9*d.*)

Reviews of the Aeronautical Research Council

1939–48 3*s.* (post 6*d.*) 1949–54 5*s.* (post 5*d.*)

Index to all Reports and Memoranda published in the Annual Technical Reports

1909–1947 R. & M. 2600 (out of print)

Indexes to the Reports and Memoranda of the Aeronautical Research Council

Between Nos. 2351–2449	R. & M. No. 2450 2*s.* (post 3*d.*)
Between Nos. 2451–2549	R. & M. No. 2550 2*s.* 6*d.* (post 3*d.*)
Between Nos. 2551–2649	R. & M. No. 2650 2*s.* 6*d.* (post 3*d.*)
Between Nos. 2651–2749	R. & M. No. 2750 2*s.* 6*d.* (post 3*d.*)
Between Nos. 2751–2849	R. & M. No. 2850 2*s.* 6*d.* (post 3*d.*)
Between Nos. 2851–2949	R. & M. No. 2950 3*s.* (post 3*d.*)
Between Nos. 2951–3049	R. & M. No. 3050 3*s.* 6*d.* (post 3*d.*)
Between Nos. 3051–3149	R. & M. No. 3150 3*s.* 6*d.* (post 3*d.*)

HER MAJESTY'S STATIONERY OFFICE

from the addresses overleaf

Printed and published by
HER MAJESTY'S STATIONERY OFFICE

To be purchased from
York House, Kingsway, London W.C.2
423 Oxford Street, London W.1
13A Castle Street, Edinburgh 2
109 St. Mary Street, Cardiff
39 King Street, Manchester 2
50 Fairfax Street, Bristol 1
35 Smallbrook, Ringway, Birmingham 5
80 Chichester Street, Belfast 1
or through any bookseller

Printed in England

S.O. Code No. 23-3357